Materials Science-Poland, *Vol. 27*, *No. 1*, *2009*

Structure and crystallization kinetics of amorphous Al–Ni–Si alloy

M. GÖGEBAKAN*, M. OKUMUS

[1]Department of Physics, Faculty of Art and Science,
Kahramanmaras Sutcu Imam University, Kahramanmaras, 46000, Turkey

In the present work, the structure and crystallization kinetics of rapidly solidified $Al_{70}Ni_{13}Si_{17}$ amorphous alloy have been investigated by a combination of differential scanning calorimetry (DSC) and X-ray diffractometry (XRD). Amorphous ribbons were obtained by melt spinning at wheel speeds higher than 10 m/s. Crystallization of amorphous $Al_{70}Ni_{13}Si_{17}$ alloy during continuous heating in DSC, takes places in three stages: (1) formation of fcc-Al and hexagonal phases; (2) growth of fcc-Al and hexagonal phases; (3) formation of fcc-Si and orthorhombic Al_3Ni phases. Isothermal annealing DSC traces for this amorphous alloy, the first crystallization peak showed a clear incubation period, and the Avrami time exponent n has been determined to be 2.4–2.8 using the Johnson–Melh–Avrami analysis. This suggested that the transformation reaction involved continuous nucleation and three dimensional diffusion-controlled growth. Electrical resistivity of the alloy was measured as 33×10^{-6} Ω·cm for the amorphous structure and 1×10^{-6} Ω·cm for the crystalline one. This study describes the structure and crystallization kinetics of a rapidly solidified $Al_{70}Ni_{13}Si_{17}$ amorphous alloy.

Key words: *amorphous alloys; rapid solidification; X-ray diffraction; calorimetry*

1. Introduction

Amorphous alloys are metallic alloys with no long range atomic order, in contrast to crystalline alloys showing long range order with a repeating unit cell. Amorphous alloys are usually produced by rapid solidification of the alloying constituents from the liquid phase at such high cooling rates that the atoms are frozen into their liquid configuration to form a metastable glass-like structure. For the last three decades, amorphous alloys have attracted great interest because of their good mechanical properties, useful physical properties and good chemical properties resulting from their new alloy composition and new atomic configurations. Particularly, great effort has

*Corresponding author, e-mail: gogebakan@ksu.edu.tr

been devoted to the production of Al-rich amorphous alloys, with the aim of utilizing a high strength material with light weight which may lead to applications in a number of fields [1–4]. Recently, Al-rich amorphous alloys have been produced in various Al–TM–RE ternary alloy systems, where TM is Fe, Co, Ni and RE is Y, La, Ce, by rapid solidification technique, and the resulting amorphous alloys exhibit high mechanical strength combined with low density, large glass-forming ability and distinctly appreciable glass transition phenomenon [5–10]. Although Al–TM–RE alloys systems could be easily amorphized by rapid solidification technique, these amorphous alloys contain expensive rare earth elements such as Y, La, Ce, and it is necessary to replace them with cheaper elements such as Si and Ni. Furthermore, the density of Si (2.3 g/cm^3) is lower than that of Y (4.45 g/cm^3), La (6.17 g/cm^3) and Ce (6.77 g/cm^3). Hence, rapidly solidified Al–Ni–Si amorphous alloys are better choice for practical application as materials with high strength, low density and useful physical properties.

In this study, we present the structure, crystallization kinetics and electrical resistivity of rapidly solidified $Al_{70}Ni_{13}Si_{17}$ amorphous alloy by a combination of differential scanning calorimetry (DSC), X-ray diffractometry (XRD) and four-probe techniques.

2. Experimental

Ternary alloy ingot with nominal composition $Al_{70}Ni_{13}Si_{17}$ (at. %) has been fabricated by melting of appropriate proportions of high purity Al, Si and Ni elements in a graphite crucible under an argon atmosphere. Rapidly solidified ribbons were manufactured by the single roller melt-spinning technique. By this technique, it is possible to quench the molten alloy at a cooling rate of 10^4–10^6 K/s. In order to obtain rapidly solidified ribbons, the ingot was re-melted in a quartz crucible and then molten alloy ejected through an orifice onto a single Cu wheel with a wheel surface velocity of 10–40 m/s. The resulting ribbons were typically 60–100 μm thick, 3–5 mm wide and up to several meters long. The amorphous/crystalline natures of the as-melt-spun and annealed ribbons were characterized by X-ray diffractometry (XRD) technique. The XRD experiments were performed using a Philips X'Pert Pro diffractometer with filtered CuK_α (λ = 0.154 nm), 35 kV and 50 mA. For phase identification, measurements were scanned for a wide range of diffraction angles (2θ) from 20° to 100° with the scanning rate of 5 deg/min. The crystallization of rapidly solidified ribbons was investigated by DSC (Perkin-Elmer DSC-7) using both continuous heating and isothermal annealing under a pure argon atmosphere. In order to ensure reliable temperature and heat release values, the DSC was calibrated using In (99.999 wt. % of pure In) and Pb (99.999 wt. % of pure Pb) standard. Continuous heating was performed at a constant heating rate of 20 K/min. Isothermal DSC measurements were carried out by annealing to various temperatures 5–15 K lower than their first crystallization peak temperatures with the heating rate of 20 K/min, and the heating duration of 3.5 h. For resistiv-

ity measurements, rapidly solidified ribbons were annealed for 30 min at various temperatures from 300 to 650 K, and then electrical resistivities of the samples were measured by the four-probe method.

3. Results and discussion

Formation of amorphous alloys by melt-spinning technique is strongly dependent on the processing parameters. The most important processing parameters are the wheel surface velocity, ejection pressure and ejection temperature. These parameters can modify the cooling rate, the viscosity of the melt and also the microstructure of the resulting ribbons. In the present work, we changed the surface velocity while keeping other parameters nominally constant. Figure 1 shows XRD spectra of the rapidly solidified $Al_{70}Ni_{13}Si_{17}$ alloys prepared using circumferential wheel speeds in the range 10–40 m/s. At the wheel speed of 10 m/s, the melt spun ribbon was very brittle and XRD trace showed the presence of peaks corresponding to elemental Al, Si phases and intermetallic Al_3Ni phases (as seen in Fig.1a). At wheel speeds greater than 10 m/s, the diffraction peaks from Al, Si and intermetallic Al_3Ni phases disappeared, and the XRD traces showed the broad halo peak indicating that the structure of the melt spun ribbon produced is amorphous.

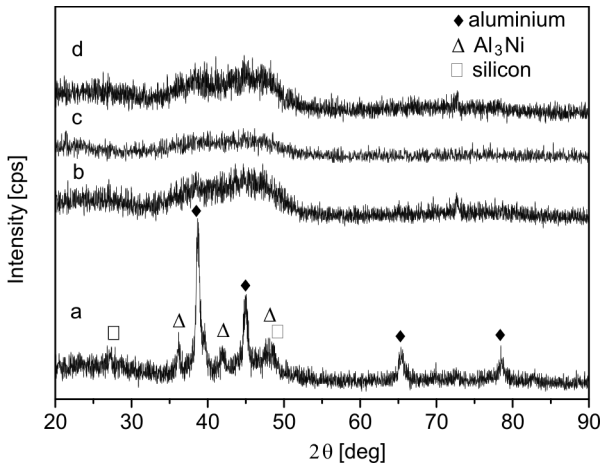

Fig. 1. XRD spectra of the $Al_{70}Ni_{13}Si_{17}$ alloys prepared at various wheel speeds: a) 10 m/s, b) 20 m/s, c) 30 m/s, and d) 40 m/s

Figure 2 shows a series of continuous DSC traces obtained from the rapidly solidified $Al_{70}Ni_{13}Si_{17}$ alloy which exhibited a broad halo peak in Fig. 1b–d. As seen in Fig. 2, the crystallization behaviour of amorphous $Al_{70}Ni_{13}Si_{17}$ alloys is very similar. The DSC traces of these amorphous alloys exhibit three exothermic peaks, indicating that structural transformation into final phase takes places in three single steps. It can

be seen that the crystallization onset temperature T_x and the first peak temperature T_1 are dependent on the wheel speed. T_x and T_1 decreased from 451 K to 442 K and from 463 K to 452 K, respectively, with increasing wheel speed from 20 m/s to 40 m/s.

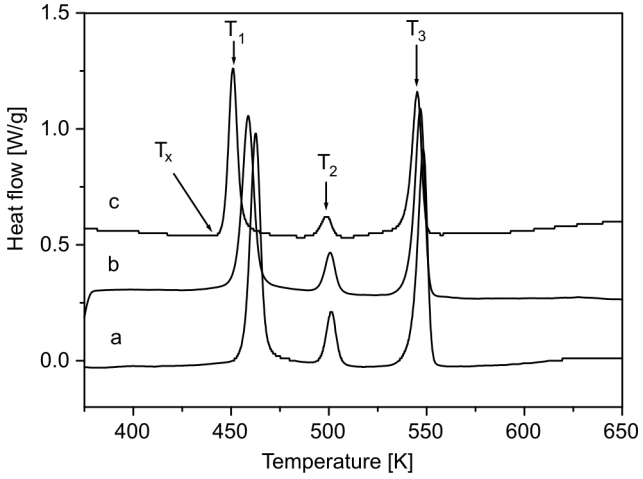

Fig. 2. Continuous DSC traces from an amorphous $Al_{70}Ni_{13}Si_{17}$ alloy manufactured at various wheel speeds: a) 20 m/s, b) 30 m/s, and c) 40 m/s

However, the crystallization peak temperature for other exothermic peaks (the second and third peak) remained constant and independent of wheel speed (Fig. 2). The crystallization onset temperature (T_x) and the three crystallization peak temperatures (T_1, T_2, T_3) are listed in Table 1.

Table 1. The crystallization onset temperature T_x and three crystallization peak temperatures T_1, T_2, T_3 of $Al_{70}Ni_{13}Si_{17}$ alloys manufactured using various wheel speeds

Wheel speed [m/s]	T_x [K]	T_1 [K]	T_2 [K]	T_3 [K]
20	451	463	501	548
30	447	459	501	547
40	442	452	500	545

The crystallization onset temperature and the three crystallization peaks temperatures are in good agreement with those reported by McKay et al. [11] for a similar alloy, as determined from their continuous DSC results. On the other hand, at temperatures below the first exothermic crystallization peak, there was no clear evidence of a glass transition effect, as would be expected for a marginal glass former. The absence of the feature characteristic of glass transition temperature could be explained assuming that during rapid solidification, a significant number of cluster distributions is formed. Under continuous heating, the clusters that are above the critical nucleation size grow even at lower temperatures. Therefore, glass transition temperature is hidden underneath the first

crystallization peak. In continuous heating analyses, the dependence of crystallization temperature on the heating rate can be used to estimate the associated crystallization activation energy by means of the Kissinger method [12]. The activation energies are presented in Table 2.

Table 2. Activation energies E_a (kJ/mol) for crystallization in $Al_{70}Ni_{13}Si_{17}$ alloys manufactured using different wheel speeds

Wheel speed [m/s]	1st peak [kJ/mol]	2nd peak [kJ/mol]	3rd peak [kJ/mol]
20	240	170	145
30	247	179	151
40	238	173	142

As seen in Table 2, the measured values of the overall activation energy for the first exothermic peaks (240±10 kJ/mol) were higher than those of the second (175±10 kJ/mol) and third exothermic peaks (145±10 kJ/mol), indicating a relatively stable amorphous structure. A similar result was reported by McKay et al [11] for Al–Ni–Si alloy. The higher activation energy implies that the energy barrier for the glass-to-crystallization phase transformation is higher, and that the amorphous structure is more stable at temperatures lower than the crystallization temperature.

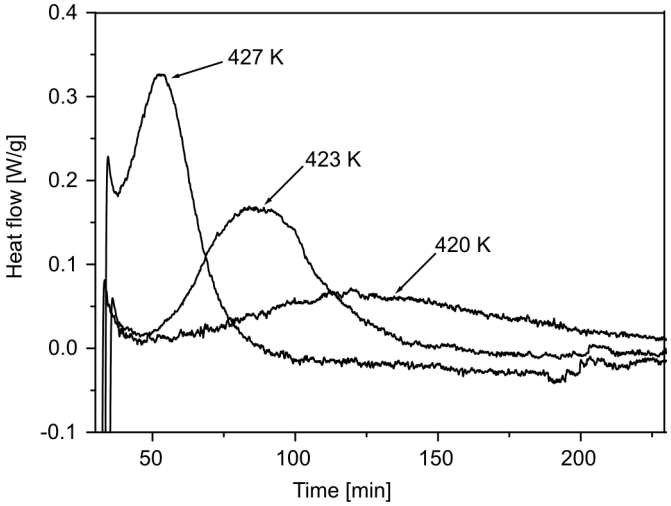

Fig. 3. DSC traces from amorphous $Al_{70}Ni_{13}Si_{17}$ alloys obtained after isothermal annealing at various temperatures

Figure 3 shows typical isothermal annealing DSC traces of amorphous $Al_{70}Ni_{13}Si_{17}$ alloy prepared at a wheel speed of 40 m/s. As seen in Fig. 3, isothermal annealing DSC traces occurred with a clear incubation period, followed by an exothermic peak. Then

a decrease in the reaction occurred, which is typical of a nucleation and growth mechanism. This suggests that the crystallization should take place by nucleation and growth, since the existence of the time dependent incubation period indicates a thermal activation nucleation barrier. The kinetics of crystallization can be expressed by the Johnson–Mehl–Avrami (JMA) equation [13] and the corresponding Avrami plots were made. This is shown in Fig. 4. From these plots, Avrami exponents n were obtained in the range 2.4–2.8. The Avrami exponent with $n = 2.5$ is associated with nucleation at a constant rate and diffusion-controlled growth [13]. Similar crystallization behaviour and Avrami exponents were reported by Gögebakan et al. for Al–Y–Ni alloy [14] and McKay et al. [11] for Al–Ni–Si alloy.

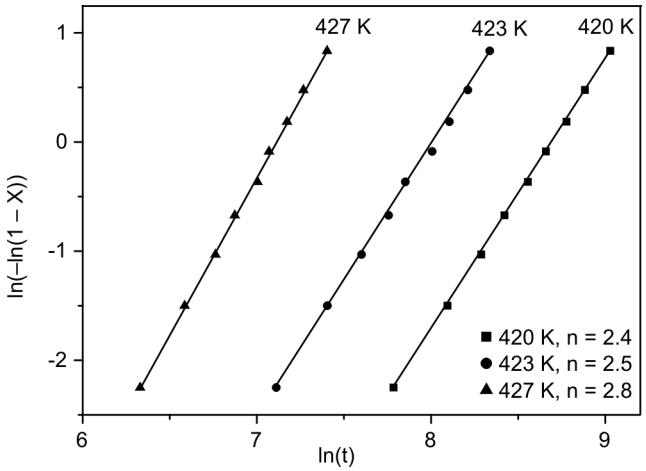

Fig. 4. Avrami plots for the amorphous $Al_{70}Ni_{13}Si_{17}$ alloy

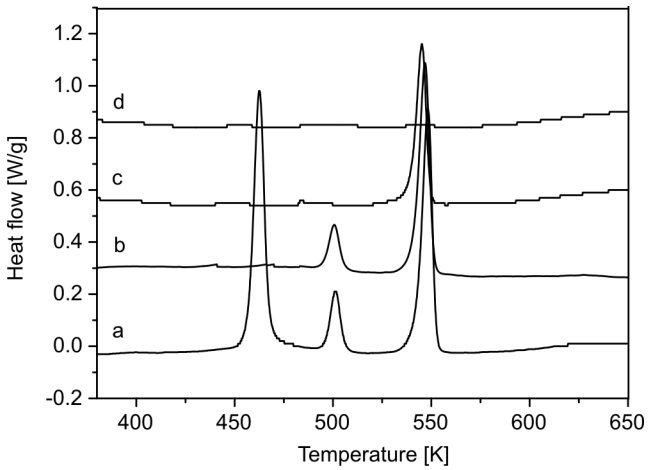

Fig. 5. DSC traces obtained during continuous heating of $Al_{70}Ni_{13}Si_{17}$ alloys as melt spun (a), and annealed for 30 min at: b) 475 K, c) 525 K, d) 575 K

To investigate the crystallization behaviour during the exothermic reactions, amorphous ribbons were heated up to the end temperatures of each exothermic reaction peak, and then cooled rapidly to freeze the microstructure for subsequent DSC and XRD analysis. Figure 5 shows a typical DSC trace obtained during continuous heating of $Al_{70}Ni_{13}Si_{17}$ alloys (prepared at a wheel speed of 40 m/s), as melt spun and annealed for 30 min at various temperatures from 475 to 575 K. The DSC traces of the as melt spun ribbon consisted of three exothermic peaks. At the annealing temperature of 475 K, the first exothermic peak disappeared and the DSC traces showed two exothermic peaks. However, the second and third exothermic peaks were not affected by the heat treatment. The DSC traces of the alloys annealed at 525 K showed only one exothermic peak. The DSC trace from alloys annealed at 575 K did not show any exothermic peak. Similar crystallization behaviour was reported by Kim et al. [4] for their Al–Y–Ni alloys.

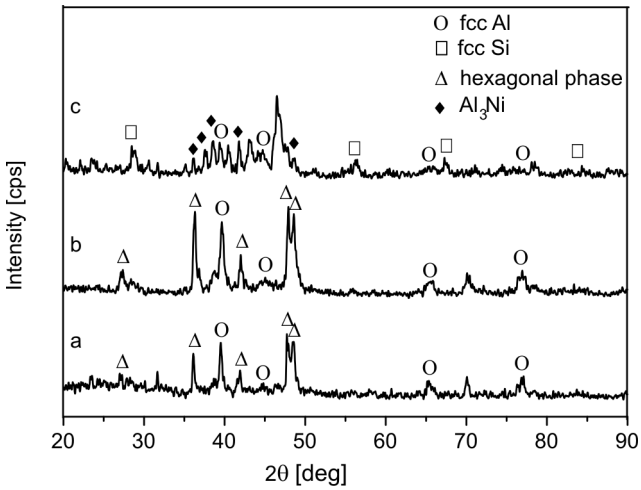

Fig. 6. XRD traces from amorphous $Al_{70}Ni_{13}Si_{17}$ alloys annealed for 30 min at: a) 475 K, b) 525 K, and c) 575 K

Figure 6 shows the XRD traces obtained from rapidly solidified $Al_{70}Ni_{13}Si_{17}$ alloys (prepared at a wheel speed of 40 m/s) after heated up to 475, 525 and 575 K, respectively. XRD results revealed that, after annealing to 475 K, fcc-Al and a hexagonal phase were formed. This hexagonal phase has been previously identified by Schumacher [15] and Legresy [16]. Therefore, this is an indication that, for amorphous $Al_{70}Ni_{13}Si_{17}$ alloys, the first crystallization peaks correspond to the formation of fcc-Al and hexagonal phases. After heating to 525 K, no new phase in the XRD traces were observed, and the intensities of present phases were increased. Therefore, the second exothermic peak in DSC corresponds to the growth of the fcc-Al and hexagonal phases. However, after annealing to 575 K, fcc-Al, fcc-Si and orthorhombic Al_3Ni phases were observed, at this stage of heating the hexagonal phase was no longer pre-

sent and this is indicating that it is metastable. This observation is in agreement with that of McKay et al [11] for Al-Ni-Si alloy.

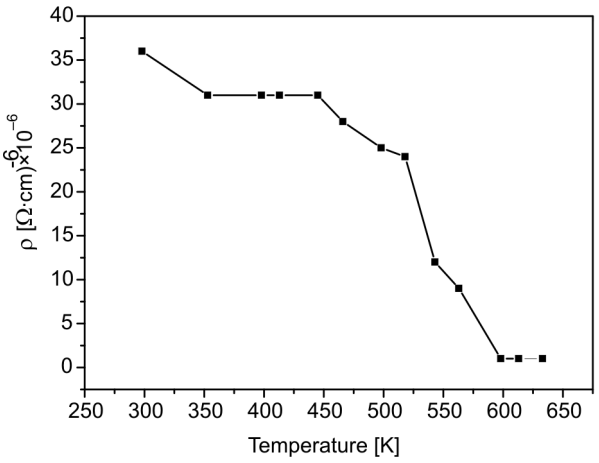

Fig. 7. Changes of electrical resistivity of $Al_{70}Ni_{13}Si_{17}$ alloys annealed at various temperatures

In order to understand the variation of the electrical resistivity with annealing temperature, amorphous ribbons were annealed for 30 min at various temperatures from 300 to 650 K. The changes in electrical resistivity with annealing temperature are shown in Fig. 7. As seen from the figure, the electrical resistivity remains nearly the same up to 450 K, which is about $33\times10^{-6}\Omega\cdot$cm. Therefore the electrical resistivity of the amorphous $Al_{70}Ni_{13}Si_{17}$ alloy is higher than that of pure Al (2.82×10^{-6} Ω·cm) and Ni (7.12×10^{-6} Ω·cm), and lower than that of Si (640×10^{2} Ω·cm). However, the highest resistivity value decreases significantly from 33×10^{-6} Ω·cm to 1×10^{-6} Ω·cm, on decompositions of the amorphous phase to a fully crystalline phase. This suggests that, in Al–Si–Ni alloy, amorphous structure is responsible for the high resistivity.

4. Conclusions

The as-spun ribbon prepared at wheel speeds higher than 10 m/s is ductile, and the XRD traces showed a broad halo peak corresponding to the amorphous structure. At the wheel speed of 10 m/s, the melt spun ribbon was very brittle and XRD trace showed the presence of peaks corresponding to elemental Al, Si phases and intermetallic Al_3Ni phase. Crystallization of amorphous $Al_{70}Ni_{13}Si_{17}$ alloy during continuous heating in DSC, takes places in three stages: (1) formation of the fcc-Al and hexagonal phases from the amorphous phase; (2) growth of the fcc-Al and hexagonal phases; (3) formation of fcc-Si and orthorhombic Al_3Ni phases. Crystallization of amorphous $Al_{70}Ni_{13}Si_{17}$ alloy during isothermal annealing at in the range 420–27 K show JMA

kinetics with the Avrami exponent of 2.4–2.8, corresponding to continuous nucleation and three dimensional diffusion-controlled growth. Electrical resistivity of the alloy was measured as 33×10^{-6} Ω·cm for the amorphous structure and as 1×10^{-6} Ω·cm for the crystalline structure.

Acknowledgements

We would like to thank the Turkish State Planning Organization (DPT) for its financial support, Project No. 103K-120-730, and Dr. Umit Alver for his technical assistance with electrical resistivity measurements.

References

[1] KIM Y.H., HIRAGA K., INOUE A., MASUMOTO T. , JO H.H., Mater. Trans. JIM., 35 (1994), 293.
[2] KIM Y.H., INOUE A. , MASUMOTO T., Mater. Trans. JIM., 31 (1990), 747.
[3] CHANG I.T.H., BOTTEN R.R., Mater. Sci. Eng. A, 226-228 (1997), 183.
[4] KIM W.T., GOGEBAKAN M., CANTOR B., Mater. Sci. Eng. A, 226–228 (1997),178.
[5] GÖGEBAKAN M., UZUN O., KARAASLAN T., KESKIN M., J. Mater. Proc. Techno., 142 (2003), 87.
[6] MUNOZ-MORRIS M.A., SURINACH S., GICH M., BARO M.D., MORRIS D.G., Acta Mater., 51 (2003), 1067.
[7] GANGOPADHYAY A.K., KELTON K.F., Philos. Mag. A, 80 (2000), 1193.
[8] BASSIM N., KIMINAMI C.S., KAUFMAN M.J., OLIVEIRA M.F., PERDIGÃO M.N.R.V., BOTTA FILHO W.J., Mater. Sci. Eng. A, 304–306 (2001), 332.
[9] GLORIANT T., PING D.H., HONO K., GREER A.L., BARO M.D., Mater. Sci. Eng. A, 304–306 (2001), 315.
[10] HONG S.J., WARREN P.J., CHUN B.S., Mater. Sci. Eng. A, 304–306 (2001), 362.
[11] MCKAY B.J., CIZEK P., SCHUMACHER P., O'REILLY K.A.Q., Mater. Sci. Eng. A, 304–306 (2001), 240.
[12] KISSINGER H.E., Anal. Chem., 29 (1957), 1702.
[13] CHRISTIAN J.W., *The Theory of Transformation in Metals and Alloys*, Pergamon Press, Oxford, UK, 1975.
[14] GÖGEBAKAN M., WARREN P.J., CANTOR B., Mater. Sci. Eng. A, 226–228 (1997), 168.
[15] SCHUMACHER P., *Nucleation in Aluminium Alloys Studied Using Devitrifation*, Ph.D. Thesis, University of Cambridge, Cambridge, UK, 1993.
[16] LEGRESY J.M., *Characterization and Kinetics of the Crystallization of Al–Ni–Si Amorphous* Alloys, Ph.D. Thesis, Institut National Polytechnique de Grenoble, 1987.

Received 8 October 2007
Revised 29 August 2008